Hierarchical Control Structure for Optimising Building Microgrid Self-consumption

Daniela Yassuda Yamashita
Université de Poitiers,
ESTIA-Recherche
Bidart, France
d.yamashita@estia.fr

Ionel Vechiu
Université de Bordeaux,
ESTIA-Recherche
Bidart, France
i.vechiu@estia.fr

Jean Paul Gaubert
Université de Poitiers,
Laboratoire d'Informatique et d'Automatique pour les Systèmes (LIAS) – ENSIP
Poitiers, France
jean.paul.gaubert@univ-poitiers.fr

***Abstract*— Renewable energy sources are increasingly deployed as distributed generators, restructuring the traditional electrical grid toward smart grids. Their intermittent power generation makes difficult the development of a complete carbon-free MicroGrid. Hence, aiming to keep the safe operation of a building MicroGrid (BMG) under stochastic variations in the power imbalance while respecting the requirements imposed by grid regulation to maximise self-consumption, a three-level energy management system was designed. The BMG main grid interaction aspects are assured by the two upper control level throughout a hierarchical model predictive control, whereas the power sharing among all electric vehicles is ensured via a deterministic state machine. The entire hierarchical control structure was tested through simulation in MATLAB under different scenarios. Results prove that the proposed control allows the BMG to keep its self-consumption index within expected boundaries despite environmental disturbances.**

Keywords*— Renewable Energy, Model Predictive Control, Electricity Market, Power sharing, self-consumption index

I. INTRODUCTION

According to [1], buildings represent one-third of global final energy consumption. Consequently, numerous policies concerning building energy efficiency have been created to improve the whole electrical grid performance. The main target is to diminish the energy loss in transmission lines by reducing electricity exchanges with the main grid [2] and foster the transition from the fuel-based grid to a smart grid composed mostly of Renewable Energy Sources (RESs) [3].

To achieve these objectives, the early concept of Building MicroGrids (BMGs), in which RESs are connected nearby the power consumption has been strongly encouraged by government financial incentives. All these investments aim to reduce building dependency on the main utility and to increase RES exploitation, either using BMG communities [4] or by independent BMGs [5].

However, BMGs which in one hand can be economically and environmentally advantageous, on the other hand increase the grid regulation complexity due to the subtle rise of electricity market actors (i.e. prosumers). Consequently, according to [6], without appropriate grid regulations, electricity price speculation and undesired grid instability may arise. For this reason, BMGs electricity market participation [2] is limited by stringent rules defined by regional regulatory commissions to motivate BMGs to consume most of its local renewable energy production, avoiding exchanging electricity with the main grid. As a result, the most important BMG requirement when trading in the electricity market is to keep both self-consumption (SC) and self-sufficiency (SS) indexes [7] indexes within adequate limits, restraining BMG to buy and sell electricity.

Besides grid regulation constraints, the widespread of BMGs is also restrained by power generation and power consumption uncertainties which make difficult the development of a reliable and profitable Energy Management System (EMS). Moreover, all building requirements must be handled by a unique EMS, even though they are not in the same time scale. In front of this problem, the Hierarchical Control (HC) structure has demonstrated suitable to manage multivariable systems with different time frames [8] as those of BMGs.There are many different types of EMS algorithms and most of them were critically reviewed in [9]. Among the existent EMS algorithms, MPC approach has demonstrated its robustness against environmental disturbances, even with linear and simplified plant model [10].

Hence, this paper presents a three-level building EMS, composed of two-level Hierarchical Model Predictive Control (HMPC) and one deterministic state machine module, for managing a BMG equipped with Li-ion batteries, a photovoltaic (PV) array and four Plug-in-Electrical Vehicles (PEVs). The proposed control's main objective is to respect building autonomy indexes boundaries defined by grid regulation policies, even with uncertainties in both power generation and power consumption. The main contribution of this paper is that it gives a full description of a hierarchical control capable of:

- Trading electricity through an aggregator.
- Responding to electricity price variation.
- Managing multiple PEV charging stations.
- Optimising building autonomy indexes (SC and SS).

The remainder of this paper is structured as follows. Section II presents the plant under study by highlighting the BMG components and its context. Section III details the proposed control strategy with its cost function and constraints. Section IV shows the main results of the proposed HC in two different scenarios, followed by a brief discussion. Finally, Section V concludes the article.

II. BMG CONTEXT AND OVERVIEW

The system under study is a grid-connected BMG, which interacts with the community aggregator, as depicted in Fig. 1. Technical specifications of each BMG component are detailed in Table I.

The building total power generation is provided either by the PVs or by purchasing electricity from the main grid. If PV power generation is higher than building demand load, the BMG can sell its surplus to the main grid according to its Levelized Cost of Energy. On the contrary, if a deficit is

verified, the BMG can purchase electricity under the community aggregator fixed price.

TABLE I. MICROGRID COMPONENTS

Component Type	Electrical specifications
Photovoltaic array	Hybrid solar panel; $P_{pv_{gen}}$: 107 kWc
Li-ion battery	C_{BAT}=120 kWh ; η_{ch}^{BAT}=0.97; η_{dis}^{BAT}=0.99; Max. Max. charge power $\left(P_{BAT}^{MAX_{spec.}}\right)$: 20 kW; Max. discharge power $(-P_{BAT}^{MIN})$: 20 kW; Min. safe SoC (SOC_{BAT}^{MIN}): 20%; Max. safe SoC (SOC_{BAT}^{MAX}): 80%;
PEV's battery	C_{PEV_i} = 41 kWh; $\eta_{ch}^{PEV_i}$=0.97; $\eta_{dis}^{PEV_i}$=0.99; $i \in$ [1; 4]; Max. charge power $\left(-P_{PEV_i}^{MAX_{ch}}\right)$: 7 kW; Max. discharge power $\left(P_{PEV_i}^{MAX_{dis}}\right)$: 7 kW; Min. safe SoC ($SOC_{PEV}^{MIN}$): 20%; Max. safe SoC ($SOC_{PEV}^{MAX}$): 80%;

Since the main objective of the hierarchical EMS (HEMS) is to maximise the BMG SC, the BMG prime interest is to exploit as much as possible the PVs and trade in the electricity market only in emergency situations. For this reason, the PV is always connected to the BMG and is controlled via the Maximum Power Point Tracking (MPPT) algorithm. Analogously, the EMS is conceived to reduce trading electricity with the main grid by charging/discharging both the Li-ion's and PEVs' batteries to match the building power consumption with PV power generation. Remarkably, PEVs can support BMG's needs, operating as elastic loads, in which their energetic demand must be satisfied within the pre-defined schedule. Therefore, through energy storage system management, the BMG must respect the limitations in selling and purchasing electricity imposed by SC and SC indexes boundaries.

Additionally, due to the low BMG energy capacity, the electricity trade with the main grid is executed indirectly by means of a community aggregator. The aggregator determines the final electricity price through an algorithm that depends on the grid power bids of each of its dependent BMGs [11]. Consequently, the community aggregator requires that each BMG sends its power bids (i.e. purchase and sell electricity) daily and hourly to determine the final electricity price of all aggregator's BMGs and then negotiate with the main grid. For this reason, in this paper, the BMG aggregator interaction was divided into two control levels: one for the daily market (MPC_1) and another for the intraday market (MPC_2). Remarkably, the final aggregator price also reflects some grid regulation signals coming from market operators, working as demand response. In this paper, peak-hours and off-peak-hours electricity prices were incorporated in the HC to shave the energy demand peak.

Another constraint that is considered in this paper is that the building EMS needs to respect the rules imposed by Capacity Allocation and Congestion Management (CACM) to avoid electricity price speculation. Therefore, two additional rules were taken into account. The first one is that only local produced energy can be sold, which means that prosumers are forbidden to sell power from their storage devices. The second one is to formulate reliable daily market (DM) bids to reduce trading in intraday market (IM). The reason behind this is that CACM requires faithful one day-ahead power exchanged planning from aggregators to mitigate the grid instability concerns [4]. Therefore, CACM charges additional taxes for short notice trades, making IM prices always higher than DM prices.

III. PROPOSED CONTROL STRATEGY

Aiming to keep adequate ranges of SC and SS indexes under PV power generation and building power consumption uncertainties, the EMS was divided into two MPCs and one Power Sharing Module (PSM), as illustrated in Fig. 1 and explained in paragraphs III-A and III-B, respectively.

A. *Two-level hierarchical MPC*

MPC optimises a pre-defined cost function each sampling time, taking into account the next state prediction to follow a desired trajectory in a future horizon composed of N samples. In this context, a comprehensive BMG model is required to predict the next state and implement the MPC. In paragraph III-A1), the battery pack, the PEVs batteries, PV power generation and building demand models are detailed, whilst in paragraph III-A2) the MPC's objective function and constraints are presented. It is noteworthy that the entire BMG was modelled using linear equations and the optimization problem was written as a Mixed Integer Programming in the MPC_1 and Mixed Integer Nonlinear Programming in MPC_2 solved in MATLAB by using the CPLEX framework of IMB®.

1) *Modelling of BMG components*

a) *Power generation and power consumption*

The PV array and the building demand load were modelled based on prediction data of forthcoming PV power generation and total power demand. Typically, the PV power generation prediction data are estimated based on weather analysis, whereas the power consumption is predicted assessing dwellings behaviour.

In this paper, the prediction data formulation was conceived by sampling measurements from th PVs installed in the building of the Laboratory of Informatics and Automation for Systems (LIAS) at the University of Poitiers

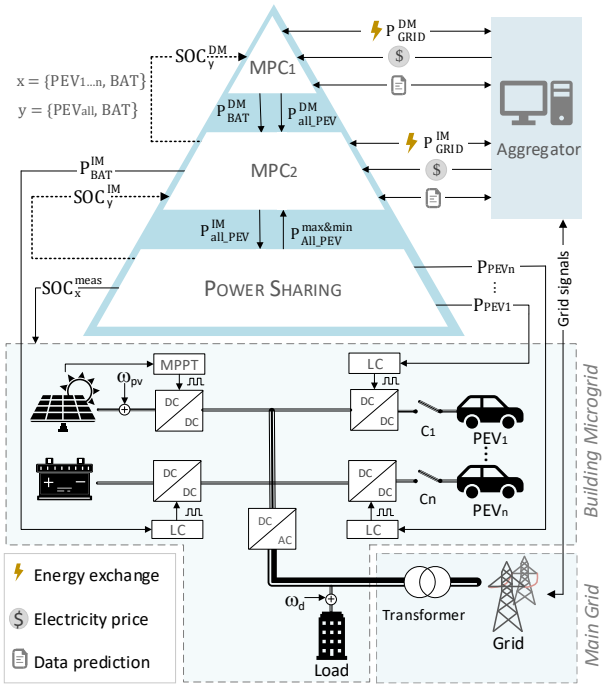

Fig. 1: Three-level HC structure for a grid-connected BMG.

in France and by collecting previous electricity bills of the Institute of Advanced Industrial Technologies (ESTIA) building. Although these data correspond to real data, they were used in the HMPC model as prediction data just for PV and building demand modelling purpose. To simulate the error in the prediction data, Gaussian disturbances were added, as pictured in Fig. 1 $(\omega_{pv}$ and $\omega_d)$.

b) Li-ion battery pack and PEVs batteries

The Li-ion battery was modelled based on its State of Charge (SoC) as considered in [10]:

$$\beta_{ch}^{j} = \left.\frac{\eta_{ch}^{j} T_s}{C_j}\right|_{j=BAT,PEV} ; \beta_{dis}^{j} = \left.\frac{T_s}{\eta_{dis}^{j} C_j}\right|_{j=BAT,PEV} \quad (1)$$

$$SOC(k+1) = SOC(k) - \beta_{ch}^{BAT} P_{BAT}^{ch}(k) - \beta_{dis}^{BAT} P_{BAT}^{dis}(k) \quad (2)$$

Where T_s is the sample time of the SoC battery discrete model and C_{BAT} is the battery capacity. Since the battery charge and discharge are not completely reversible, it was considered different efficiencies (η_{ch} and η_{dis}) when injecting (P_{BAT}^{ch}) or extracting (P_{BAT}^{dis}) active power.

Similarly, the PEVs batteries dynamic was calculated based on the average SoC of all PEVs, instead of modelling each PEV individually. Therefore, their total storage energy (E_{PEV}) is calculated as in [12]:

$$E_{PEV}(k+1) = \gamma(k) E_{PEV}(k) - \beta_{ch}^{PEV} P_{PEV}^{ch}(k) - \beta_{dis}^{PEV} P_{PEV}^{dis}(k) + SOC_{PEV}^{initial} C_{PEV} N_{PEV}^{arr}(k) \quad (3)$$

$$\gamma(k) = \begin{cases} 1 - N_{PEV}^{dep}(k)/N_{PEV}(k), if\ N_{PEV}(k) > 0 \\ 0 \qquad\qquad\qquad\quad , otherwise \end{cases} \quad (4)$$

$N_{PEV}^{arr}(k)$ and $N_{PEV}^{dep}(k)$ represent the number of PEVs that arrived and departed at instant k, respectively. These two deterministic variables are calculated from the total number of PEVs connected at instant k ($N_{PEV}(k)$).

2) MPC's objective functions and constraints

a) MPC₁: Economical Model Predictive Control

The upper level, named here as MPC₁, is mainly responsible for determining the amount of energy to be traded into the DM in the following day (P_{grid}^{DM}). It also determines the power reference of charge and discharge of the battery pack (P_{BAT}^{DM}) and the average PEVs batteries ($P_{all\ PEV}^{DM}$). The MPC₁ module receives as input the PV power generation (P_{PV}^{DM}), the resident power consumption (P_{cons}^{DM}) and the number of PEVs plugged to the BMG (N_{PEV}) prediction data with a horizon of N_h^{DM}. The MPC₁ updates its prediction data at each T_s^{DM}, which is discretized into T'^{DM}_s.

The main role of MPC₁ is to determine batteries power references and the active power grid commitment in the daily market $(\theta_{MPC_1} = [P_{BAT}^{DM}, P_{all\ PEV}^{DM}, P_{grid}^{DM}])$ for each slot time $k_2 \in [1; N_h^{DM}]$ that:

- $\boldsymbol{J_1}$**:** minimize grid energy exchange in the DM.
- $\boldsymbol{J_2}$**:** charge all PEVs before the end of the day.
- $\boldsymbol{J_3}$**:** maximize the self-consumption index (α_{sc}^{DM})

To assure these objectives, in each step time (T_s^{DM}) the MPC₁ minimises the following cost function:

$$\min_{\theta_{MPC_1}} J_{MPC_1} = \sum_{k_1=1}^{N_h^{DM}} J_1(k_1) + J_2(k_1) + J_3(k_1) \quad (5)$$

$$J_1(k_1) = \omega_1^{DM,k_1} P_{grid}^{DM_{pur}}(k_1) - \omega_2^{DM,k_1} P_{grid}^{DM_{sell}}(k_1) \quad (6)$$

$$J_2(k_1) = \omega_3^{DM,k_1} E_{PEV}(k_1) \quad (7)$$

$$J_3(k_1) = \omega_4^{DM,k_1} \alpha_{sc}^{DM}(k_1) \quad (8)$$

Remarkably, the electricity price embedded in J_1 $(\pi_{pur}^{DM}$ and $\pi_{sell}^{DM})$ reflects the demand response signal coming from the aggregator to reduce the power consumption in peak hours. Therefore, from 7 AM to 8 PM, the electricity price π_{pur}^{DM} is about 30% more expensive than off-peak periods, while π_{sell}^{DM} is kept constant all along the day. The factors ω_1^{DM,k_1}, ω_2^{DM,k_1}, ω_3^{DM,k_1} and ω_4^{DM,k_1} are to normalise the cost functions and guarantee that the pre-defined multi-objective priority order is satisfied.

Charging the PEVs is considered a high priority objective, followed by maximising SC rate and minimising the exchanges with the main grid. Consequently, in the case of deficit, it is expected that the BMG purchases electricity from the main grid to assure that all PEVs are charged at the end of the day, even though it will raise the total energy costs and penalise the self-efficiency index.

The objective function defined in (5) – (8) is subject to equality and inequality constraints to respect the grid regulation rules previously mentioned. To guarantee the BMG safe operation, the power balance must always be satisfied. For this reason, equality equations (9) – (13) are imposed to MPC₁, where $P_{grid}^{DM_{sell}} < 0$ and $P_{grid}^{DM_{pur}} > 0$ correspond to the amount of energy to be sold and purchased in DM. The prediction of the future state variables, which is based on the dynamic model equations (2) and (3), are also incorporated in the equality constraints as well as the SC rate calculation stated in (13).

$$P_{imb}^{DM}(k_1) = P_{cons}^{DM}(k_1) - P_{PV}^{DM}(k_1) \quad (9)$$

$$P_{imb}^{DM}(k_1) = P_{grid}^{DM}(k_1) + P_{BAT}^{DM}(k_1) + P_{allPEV}^{DM}(k_1) \quad (10)$$

$$P_{PEV}(k_1) = P_i^{ch}(k_1) + P_i^{dis}(k_1)|_{i=BAT,PEV} \quad (11)$$

$$P_{grid}^{DM}(k_1) = P_{grid}^{DM_{sell}}(k_1) + P_{grid}^{DM_{pur}}(k_1) \quad (12)$$

$$\alpha_{sc}^{DM}(k_1) = 1 + \sum_{k_1=1}^{N_h^{DM}} P_{grid}^{DM_{sell}}(k_1) \Big/ \sum_{k_1=1}^{N_h^{DM}} P_{PV}(k_1) \quad (13)$$

Since in the real system, it is not possible to neither charge and discharge the battery nor purchase and sell electricity at the same time, integer variables were incorporated into inequality constraints working as mixed logic dynamic constraints as presented in [10]. Still considering the BMG safe operation, it is essential to respect the electrical component manufacture datasheet (summarised in Table I) to extend the lifetime of MG's distributed energy resources. Therefore, for each state and control variables $x_{DM}(k_1)$, boundary constraints are written as specified in the following general equation.

$$x_{DM}^{MIN} \leq x_{DM}(k_1) \leq x_{DM}^{MAX} \quad (14)$$

b) MPC₂: Tracking Model Predictive Control

The middle level, called here as MPC₂, tries to follow both Li-ion and PEV battery power reference calculated by MPC₁ module. The MPC₂ has three output signals. One

signal is conceived to specify the building IM bids $\left(P_{grid}^{IM}\right)$ and is sent toward the community aggregator. The second signal corresponds to the power reference for Li-ion battery pack (P_{BAT}^{IM}), that is sent directly to the real system. The last signal is the average PEVs batteries power reference ($P_{all\ PEV}^{IM}$) that is transmitted to the PSM. The MPC$_2$ module receives the same inputs as MPC$_1$ (P_{PV}^{DM}, P_{cons}^{DM} and N_{PEV}), but more periodically (T_s^{IM}) and more short-sightedly (N_h^{IM}) than MPC$_1$. As a result, the MPC$_2$ has more accurate data than the upper layer, which enables it to correct the power references toward the real BMG and reduce the drawbacks provoked by data prediction uncertainties.

The MPC$_2$'s objective is divided into four major objectives to determine the corrective control variables $\left(\theta_{MPC_2} = \left[P_{BAT}^{IM}, P_{all\ PEV}^{IM}, P_{grid}^{IM}\right]\right)$ in each slot time $k_2 \in [1; N_h^{IM}]h$:

- $\boldsymbol{J_1}$**:** Track Li-ion battery pack power references.
- $\boldsymbol{J_2}$**:** Track PEV's battery power references.
- $\boldsymbol{J_3}$**:** Minimize grid energy exchange in the IM.
- $\boldsymbol{J_4}$**:** Charge all the PEVs before their departure.

To accomplish these objectives, the MPC$_2$ minimises at each step time (T_s^{IM}) the following cost function.

$$\min_{\theta_{MPC_2}} J_{MPC_2} = \sum_{k_2=1}^{N_h^{IM}} J_1(k_2) + J_2(k_2) + J_3(k_2) + J_4(k_2) \quad (15)$$

$$J_1(k_2) = \omega_1^{IM}\left(P_{BAT}^{DM}(k_2) - P_{BAT}^{IM}(k_2)\right)^2 \quad (16)$$

$$J_2(k_2) = \omega_2^{IM}\left(P_{PEV}^{DM}(k_2) - P_{PEV}^{IM}(k_2)\right)^2 \quad (17)$$

$$J_3(k_2) = \omega_3^{IM,k_2}\, P_{grid}^{IM_{pur}}(k_2) - \omega_4^{IM,k_2}\, P_{grid}^{IM_{sell}}(k_2) \quad (18)$$

$$J_4(k_2) = -\omega_5^{IM,k_2} E_{PEV}(k_2) \quad (19)$$

Where ω_1^{IM}, ω_2^{IM}, ω_3^{IM,k_2}, ω_3^{IM,k_2} and ω_5^{IM,k_2} define the priority order of the multi-objective cost function, making J_4 to be satisfied firstly, followed by J_2, J_1 and J_3. In (19), the value of ω_5^{IM,k_2} depends on the estimated departure time of most of PEVs. The nearer the departure time is from k_2, the higher ω_5^{IM,k_2}.

As in the upper level, the equality constraints are fundamental to assure the BMG power imbalance and to model the system behaviour. However, the power balance is calculated slightly different from the MPC$_1$ because it considers the grid commitment in the daily market as an energy provider, as formulated in (20) and (21). However, the inequality constraints and boundary constraints were designed similarly to MPC$_1$.

$$P_{imb}^{IM}(k_2) = P_{cons}^{IM}(k_2) - P_{PV}^{IM}(k_2) - P_{grid}^{DM}(k_2) \quad (20)$$

$$P_{grid}^{IM}(k_2) + P_{BAT}^{IM}(k_2) + P_{allPEV}^{IM}(k_2) = P_{imb}^{IM}(k_2) \quad (21)$$

B. Power Sharing Module

In the lower control level, named here as PSM, a deterministic state machine shares the average power reference $P_{all\ PEV}^{IM}$ coming from MPC$_1$ among each PEV battery based on their current SoC. The PSM divide P_{PEV}^{IM} among the four PEVs charging stations so that to charge all PEVs at the end of the day. Since the number of equations rises according to the N_{PEV}^{IM}, a state machine was developed rather than incorporating it into the existent MPC$_2$ module. Basically, each PEV power reference is calculated based on the current SoC measurement $\left(s_{i,k} = SOC_{PEV_{i\in\mathcal{C}_k}}^{k}\right)$, forming the subset $\mathcal{S}_k = \left\{s_{i,k} \middle| \forall i \in [1;4]\right\}$. Where $\mathcal{C}_k$ is the subset containing all the PEVs connected at instant k. It also depends on the average ($\bar{m} = mean(\mathcal{S}_k)$), maximum ($v_{dis} = max(\mathcal{S}_k)$)and minimum ($v_{ch} = min(\mathcal{S}_k)$) of SoC of all PEV connected at instant k. Contrary to MPC$_2$, the PSM considers the maximum power allowed for each PEV. Therefore, at each step, the PSM updates the maximum and minimum power of the MPC$_2$ average power reference ($P_{PEV}^{max\&min}$ in Fig. 1), by using the equation (22):

$$P_{PEV_i}^{MAX_j} = \sum_{i=1}^{N_{PEV_k}} min\left(P_{PEV_i}^{MAX_j}, \frac{\left(v_j - SOC_{PEV_i}^{k+1}\right)}{\beta_{ch}}\right)\Bigg|_{j=ch,dis} \quad (22)$$

Where $SOC_{PEV_i}^{k+1}$ is the estimated PEV_i SoC at $k+1$ using the P_{PEV_i} calculated in the power-sharing state machine interaction and the battery model (2). Therefore, the main steps of the PSM are:

1. Measure N_{PEV_k} and $s_{i,k}$.
2. Determine v_{ch}, v_{dis} and $\bar{m}$.
3. Calculate the power reference of each PEV $\left(\mathcal{P} = \left\{P_{PEV_{\forall i\in\mathcal{C}_k}}\right\}\right)$ using equations (23) – (27).
4. Verify the feasibility of the result. If $\mathcal{P}$ is a valid solution (i.e. all $P_{PEV_i}^{MAX_{ch}} \le P_{PEV_{\forall i\in\mathcal{C}_k}} \le P_{PEV_i}^{MAX_{dis}}$ and all $SOC_{PEV}^{MIN} \le SOC_{PEV_{\forall i\in\mathcal{C}_{k+1}}} \le SOC_{PEV}^{MAX}$) send the result to the real system, otherwise repeat steps 1 to 3 with $P_{PEV_{\forall i\in\mathcal{C}_k}}$ boundary limitation.

The power-sharing of P_{PEV}^{IM} is composed of two parts: a common part that is equal for all PEV $\left(P_{PEV_i}^{com}\right)$ and an individual part $\left(P_{PEV_i}^{ind}\right)$ that depends on the distance either between the SOC_{PEV_i} and v_{ch} in the charging mode or between the SOC_{PEV_i} and v_{dis} in discharging mode.

$$P_{PEV_{i,k}}^{com} = P_{PEV_k}^{IM}(1 - \alpha_k / N_{PEV_k}) \quad (23)$$

$$P_{PEV_{i,k}}^{ind} = \alpha_k P_{PEV_{i,k}}^{IM} |v_j - s_{i,k}| \Big/ \sum_{i\in\mathcal{C}_k} |v_j - s_{i,k}| \Big|_{j=ch,dis} \quad (24)$$

$$P_{PEV_{\forall i\in\mathcal{C}_k}} = P_{PEV_{i,k}}^{com} + P_{PEV_{i,k}}^{ind} \quad (25)$$

$$SOC_{target,k}^{k} = \bar{m} + P_{PEV_k}^{IM} \cdot \beta_j^{PEV}\Big|_{j=ch,dis} \quad (26)$$

$$\alpha_k = \frac{|v_j - SOC_{target}^{k}|}{\left(P_{PEV}^{IM^k} \cdot \beta_{ch,dis}^{PEV}\right) - \frac{1}{N_{PEV_k}}} \cdot \frac{1}{-\frac{1}{N_{PEV_k}} + \frac{(M^k - m^k)}{\sum_{i\in\mathcal{C}_k} |v_j - s_i^k|}}\Bigg|_{j=ch,dis} \quad (27)$$

IV. Simulation Results and Discussion

To demonstrate the robustness of the developed HC, $47h$ were simulated under two different scenarios. The first one (Case A) is an ideal scenario where no disturbance was considered, whereas the second one (Case B) is a more realistic case, where uncertainties in data prediction were taken into account. Remarkably, in both scenarios, all PEVs connections were considered deterministic with well-known arrival and departure time. This assumption is aligned with the reality because the PEVs charging stations allow PEVs'

users to schedule their connections as soon as they plug their PEVs to the BMG.

The MPC_1 horizon is $N_h^{DM} = 48h$, and the data prediction is updated each $T_s^{DM} = 24h$. Therefore, 72 h of prediction data discretised into $T'^{DM}_s = 1h$ are needed. Likewise, MPC_2 posses a horizon of $N_h^{IM} = 6h$ and optimises its cost function each $T_s^{IM} = 1h$. Fig. 2 shows the one-hour-step profile of the PV power generation prediction data used in this study, which correspond to a cloudy followed by a completely sunny and one partially sunny day. Analogously, the building demand is identical during the three days, with two energy demand peaks per day : the first one from 6 AM to 10 AM, followed by a second peak between 4 PM and 7 PM.

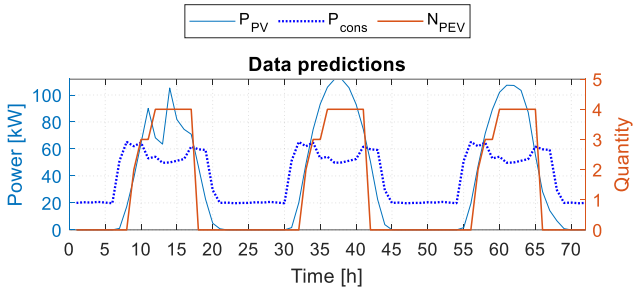

Fig. 2: Data prediction of PV power generation (P_{PV}), building power consumption (P_{cons}) and number of PEVs plugged to the BMG (N_{PEV}).

The HC's main objective is to respect the French's Energy Regulatory Commission recommendation to encourage SC for BMGs in France, in which all buildings must keep the SC index $\alpha_{sc} \geq 80\%$ and the SS index $\alpha_{ss} \geq 30\%$. In other words, over a year, the BMG must sell up to 20% of PV power generation and buy up to 70% of its total power consumption.

A. *Case A:HMPC without any disturbance*

The first case of study is an ideal scenario in which the data prediction is completely compliant with the real solar irradiation and the real power demand. Furthermore, it was considered that all PEVs arrived with a SoC of 20%, as shown in Fig. 3a. From Fig. 4c, it can be noted that the battery SoC in MPC_1 (SOC^{DM}) is almost the same in MPC_2(SOC^{IM}). This result is expected because it is an ideal case, where the day ahead data prediction is the same as those one hour before. Consequently, the MPC_2 achieves to follow the power references calculated by MPC_1 reducing the amount of energy traded in IM, leading MPC_2 optimal solution to be nearly the same as those in MPC_1.

The small differences between SOC^{DM} and SOC^{IM} are because the MPC_1 does not consider individual PEVs SoC boundaries, whereas the MPC_2 limits P_{PEV}^{IM} according to $P_{PEV}^{max\&min}$ from PSM. This situation happened at $35h$, $36h$ and $38h$, where the P_{BAT} and P_{PEV} reached their maximum ($|P_{BAT}| = 20kW$ or $P_{PEV} = P_{PEV}^{max\&min}$). Therefore, the MPC_2 had to trade electricity in the IM. In Fig. 4, the battery packs are charged only in peak-hours energy demand, due to the restriction to charge the BMG storage devices only from PVs. However, when there is no PV power generation and purchasing electricity price is more expensive (peak-hours), the batteries are discharged to reduce the electricity bill, as pictured in Fig.4a and Fig. 4b.

Notably, both autonomy indexes were kept within the recommended boundaries, i.e. $\alpha_{sc} \geq 80\%$.and $\alpha_{ss} \geq 30\%$,

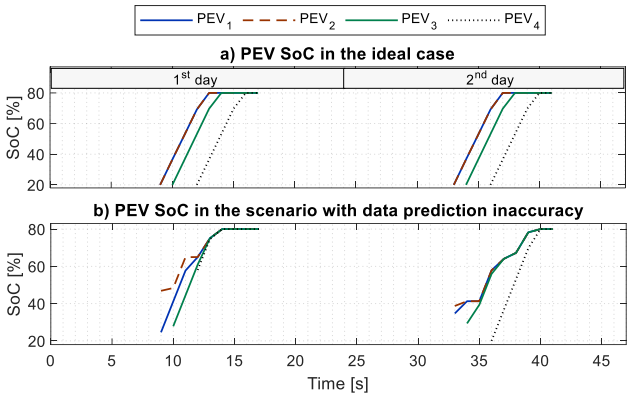

Fig. 3: State of charge of each PEV. (a) Ideal case without any disturbance (Case A). (b) Case with error in data prediction (Case B).

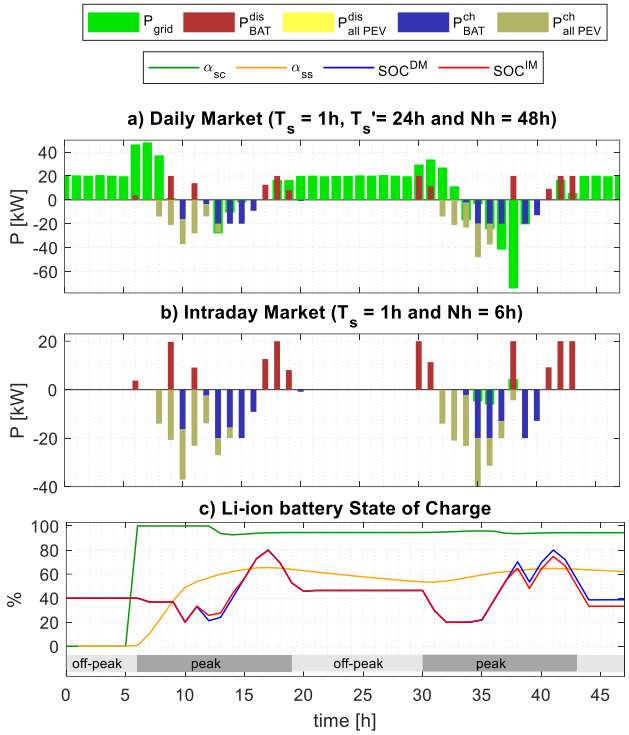

Fig. 4: HMPC without any disturbance. (a) MPC_1 variables in DM time frame. (b) MPC_2 variables in IM time frame. (c) Li-ion batteries SoC, self-consumption and self-sufficiency index in the two days.

without discharging or shifting PEVs to support the BMG. Although all PEVs are not plugged to the BMG at the same time, the PSM achieved to charge all PEVs to 80%.

B. *Case B:HMPC with disturbances*

To verify the impact of prediction error data in the building autonomy indexes, a Gaussian disturbance of mean $2kW$ and a standard deviation of 4 kW was introduced in the PV power generation (ω_{pv}). and in the building demand (ω_d). Moreover, the initial PEV battery SoC was modelled as a random Gaussian variable with mean 30% and standard a deviation of 15 %, as illustrated in the Fig. 3b.

Due to differences in the data prediction in MPC_1 and MPC_2, the state variables SOC^{DM} and SOC^{IM} are no more the same. Each multiple of $24h$, the MPC_1 state variables are updated. For this reason, only the first $23h$, the SOC^{DM} in Fig. 4c and Fig. 5c are equivalent. Afterward, the MPC_1 updates its knowledge and try to determine the best control variables. However, due to the disturbances ω_d and ω_{pv},the MPC_2 had to purchase electricity in the IM, decreasing

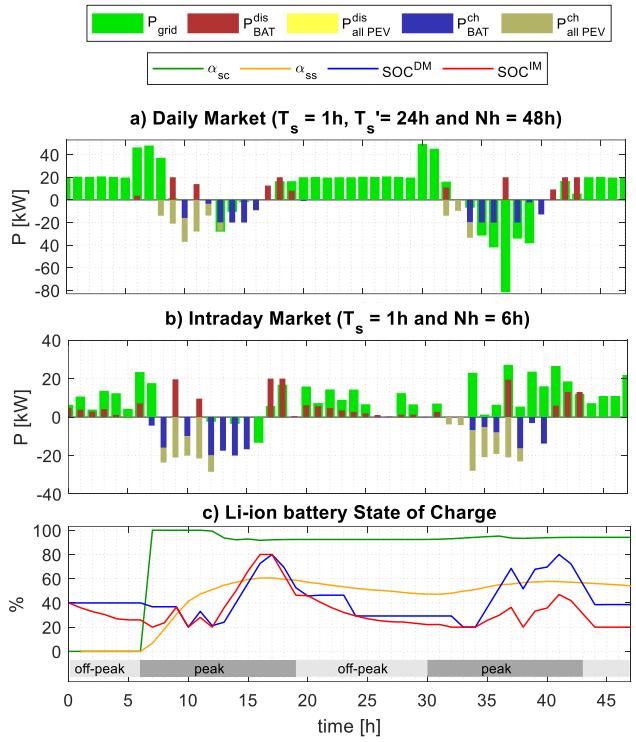

Fig. 5: HMPC with disturbances. (a) MPC1 variables in DM time frame. (b) MPC2 variables in IM time frame. (c) Li-ion batteries SoC, self-consumption and self-sufficiency index in the two days.

TABLE II. HIERARCHICAL CONTROL MAIN RESULTS

Case	α_{sc} [%]	α_{ss} [%]	Total power purchased [c]		Total power sold [c]		Total PV_{gen} [c]
			IM	DM	IM	DM	
A	92.7[a] 94.7[b]	53.4 [a] 60.8 [b]	4.4	693.4	11.1	222.4	1684
B	91.7[a] 93.8[b]	47.2 [a] 54.0 [b]	419.4	702.5	19.5	275.4	1583

[a]Minimum [b]Average [c] [kW]

α_{ss} slightly, as compared in Table II.

To reduce exchanging electricity with the main grid, the MPC_2 did not follow the P_{BAT}^{DM} coming from MPC_2. As a result, the Li-ion battery pack was less charged, ending the day with SoC around 25% instead of 40% in case A. In Fig. 3b, some PEVs charging schedules were shifted to support the BMG. Furthermore, despite the random PEV initial SoC, the PSM achieved to charge all the four PEVs to 80%.

In Fig. 5c, it can be observed that at $12h$, $14h$ and $16h$ the BMG was obligated to sell electricity in IM market because the BMG had an unexpected power surplus that neither the Li-ion nor PEV batteries could absorb due to either physical constraint of the maximum power rate or full batteries charge ($SOC = 80\%$). Since the difference in the total electricity sold is insignificant compared to the entire PV power production, the α_{sc}in Case B is pratically equal to α_{sc} in Case A. In Case B, the BMG had to purchased more electricity in the IM, wich lead a reduction of about 6% in the SC.

V. CONCLUSION

This paper aims to demonstrate the feasibility of a hierarchical control structure in a medium-size office building MicroGrid. To keep the building autonomy indexes within expected boundaries under data prediction uncertainties, the energy management system was divided into three hierarchical control layers. The economic aspect was integrated as the main factor in the two-layer model predictive control optimisations, while a state machine assures the power-sharing. The results demonstrate that under external disturbances, the proposed control is capable of keeping the self-consumption index higher than 80% and self-sufficiency index greater than 30% during two days of simulation. Consequently, if every day both indexes are maintained within the recommended limits, the requirement during an entire year will also be satisfied. After the simulations, it was proved that the proposed hierarchical control could also guarantee that all PEVs be charged before their departure time, even though some of them were shifted in time to support BMG. Further work will focus on keeping adequate building autonomy indicator rates along an entire year, by adding a hydrogen storage system to cover the deficit of energy production during the winter. Additionally, modules to soften the effects of data prediction uncertainties will be investigated.

ACKNOWLEDGEMENT

The authors would like to thank Region Nouvelle Aquitaine (research agreement: AAPFO424953) and ESTIA, the Institute of Advanced Industrial Technologies, for their financial support for the OptiMicroGrid project.

REFERENCES

[1] "Renewables 2018 Global Status Report." Renewable Energy Policy Network for the 21st Century, 2018.

[2] J. Hu, R. Harmsen, W. Crijns-Graus, E. Worrell, and M. van den Broek, "Identifying barriers to large-scale integration of variable renewable electricity into the electricity market: A literature review of market design," *Renew. Sustain. Energy Rev.*, vol. 81, pp. 2181–2195, Jan. 2018.

[3] T. M. Lawrence *et al.*, "Ten questions concerning integrating smart buildings into the smart grid," *Build. Environ.*, vol. 108, pp. 273–283, Nov. 2016.

[4] P. Tian, X. Xiao, K. Wang, and R. Ding, "A Hierarchical Energy Management System Based on Hierarchical Optimization for Microgrid Community Economic Operation," *IEEE Trans. Smart Grid*, vol. 7, no. 5, pp. 2230–2241, Sep. 2016.

[5] X. Jin, J. Wu, Y. Mu, M. Wang, X. Xu, and H. Jia, "Hierarchical microgrid energy management in an office building," *Appl. Energy*, vol. 208, pp. 480–494, Dec. 2017.

[6] H. Ren, Q. Wu, W. Gao, and W. Zhou, "Optimal operation of a grid-connected hybrid PV/fuel cell/battery energy system for residential applications," *Energy*, vol. 113, pp. 702–712, Oct. 2016.

[7] R. Luthander, J. Widén, D. Nilsson, and J. Palm, "Photovoltaic self-consumption in buildings: A review," *Appl. Energy*, vol. 142, pp. 80–94, Mar. 2015.

[8] A. M. R. Lede, M. G. Molina, M. Martinez, and P. E. Mercado, "Microgrid architectures for distributed generation: A brief review," in *2017 IEEE PES Innovative Smart Grid Technologies Conference - Latin America (ISGT Latin America)*, 2017, pp. 1–6.

[9] M. F. Zia, E. Elbouchikhi, and M. Benbouzid, "Microgrids energy management systems: A critical review on methods, solutions, and prospects," *Appl. Energy*, vol. 222, pp. 1033–1055, Jul. 2018.

[10] F. Garcia-Torres and C. Bordons, "Optimal Economical Schedule of Hydrogen-Based Microgrids With Hybrid Storage Using Model Predictive Control," *IEEE Trans. Ind. Electron.*, vol. 62, no. 8, pp. 5195–5207, Aug. 2015.

[11] R. Lu, S. H. Hong, and X. Zhang, "A Dynamic pricing demand response algorithm for smart grid: Reinforcement learning approach," *Appl. Energy*, vol. 220, pp. 220–230, Jun. 2018.

[12] M. Tavakoli, F. Shokridehaki, M. Marzband, R. Godina, and E. Pouresmaeil, "A two stage hierarchical control approach for the optimal energy management in commercial building microgrids based on local wind power and PEVs," *Sustain. Cities Soc.*, vol. 41, pp. 332–340, Aug. 2018.